User-Centric Interactive AI for Distributed Diffusion Model-based AI-Generated Content

Hongyang Du, Ruichen Zhang, Dusit Niyato, *Fellow, IEEE*, Jiawen Kang, Zehui Xiong,
Shuguang Cui, *Fellow, IEEE*, Xuemin (Sherman) Shen, *Fellow, IEEE*, and Dong In Kim, *Fellow, IEEE*

◆

Abstract—Distributed Artificial Intelligence-Generated Content (AIGC) has attracted increasing attention. However, it faces two significant challenges: how to maximize the subjective Quality of Experience (QoE) and how to enhance the energy efficiency, which are particularly pronounced in widely adopted Generative Diffusion Model (GDM)-based AIGC services for image generation. In this paper, we propose a novel user-centric Interactive AI (IAI) approach for service management, with a distributed GDM-based AIGC framework, prioritizing efficient and collaborative GDM deployment. Specifically, we restructure the GDM's inference process, i.e., the denoising chain, to enable users' semantically similar prompts to share a portion of diffusion steps. Furthermore, to maximize the users' subjective QoE, we propose a IAI approach, i.e., Reinforcement Learning With Large Language Models Interaction (RLLI), which utilizes Large Language Model (LLM)-empowered generative agents to replicate users interaction, providing real-time and subjective QoE feedback that reflects a spectrum of user personalities. Lastly, we present the GDM-based Deep Deterministic Policy Gradient (G-DDPG) algorithm, adapted to the proposed RLLI framework, for effective communication and computing resource allocation while considering user subjective personalities and dynamic wireless environments in decision-making. Simulation results show that G-DDPG can increase the sum QoE by 15%, compared with the conventional DDPG algorithm.

Index Terms—AI-generated content, reinforcement learning, generative diffusion model, generative agents, large language models

1 INTRODUCTION

THE demand for artificial intelligence-generated content (AIGC) services in areas including multimedia and business [1] is propelled by advanced generative AI (GAI)

H. Du, R. C. Zhang, and D. Niyato are with the School of Computer Science and Engineering, Nanyang Technological University, Singapore (e-mail: hongyang001@e.ntu.edu.sg, ruichen.zhang@ntu.edu.sg, dniyato@ntu.edu.sg).
J. Kang is with the School of Automation, Guangdong University of Technology, China. (e-mail: kavinkang@gdut.edu.cn)
Z. Xiong is with the Pillar of Information Systems Technology and Design, Singapore University of Technology and Design, Singapore (e-mail: zehui_xiong@sutd.edu.sg)
S. Cui is with the School of Science and Engineering (SSE) and the Future Network of Intelligence Institute (FNii), Chinese University of Hong Kong (Shenzhen), China (e-mail: shuguangcui@cuhk.edu.cn).
X. Shen is with the Department of Electrical and Computer Engineering, University of Waterloo, Waterloo, ON N2L 3G1, Canada (e-mail: sshen@uwaterloo.ca).
D. I. Kim is with the Department of Electrical and Computer Engineering, Sungkyunkwan University, Suwon 16419, South Korea (email:dikim@skku.ac.kr).
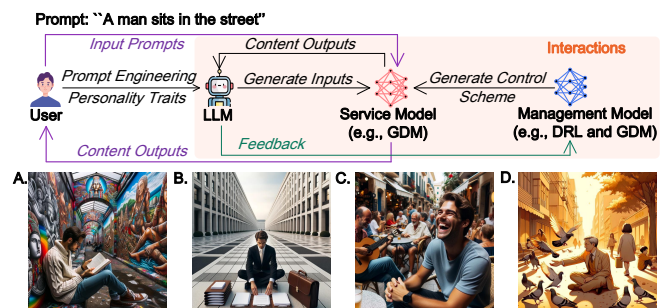
Fig. 1. The basic framework of interactive AI and four images generated with the prompt *"A man sits in the street"*. **Part A** is a man engrossed in a book against vibrant street art appeals to users with high *openness*. **Part B** is a formally dressed man on a clean street, resonating with users high in *conscientiousness*. **Part C** is a sociable street cafe scene, suitable for users with high *extraversion*. **Part D** is a man feeding pigeons in a peaceful setting with playing children, fitting for users with high *agreeableness*.

models, which offer scalable and consistent output in text and imagery [2]. For instance, ChatGPT attracted more than 100 million active users within two months [3], highlighting its impact on text-based interactions [3]. In the realm of visual content generation, Stable Diffusion's capacity to create images from text prompts shows significant progress in multi-modal technologies [4], [5]. The widespread adoption of AIGC services in human societies indicates a notable transition to Interactive AI (IAI) as the next evolutionary phase of GAI [6]. This shift is redefining how humans interact with content and underscores the dynamic progression in human-AI interaction.

However, Quality of Experience (QoE) maximization in AIGC services emerges as a critical challenge, due to the subjective nature of human perception, which extends beyond objective image quality metrics [7], [8]. Four images in Fig. 1 exemplify this complexity, showing four distinct images that are generated under a same prompt *"A man sits in the street"*. Although each image is of high quality, these images cater to different personality profiles, affecting QoE evaluations variably. Thus, network designers aspire to develop service models and service management models tailored to individual user personalities to maximize QoE. However, the absence of a definitive mathematical model for QoE complicates this optimization process. While some
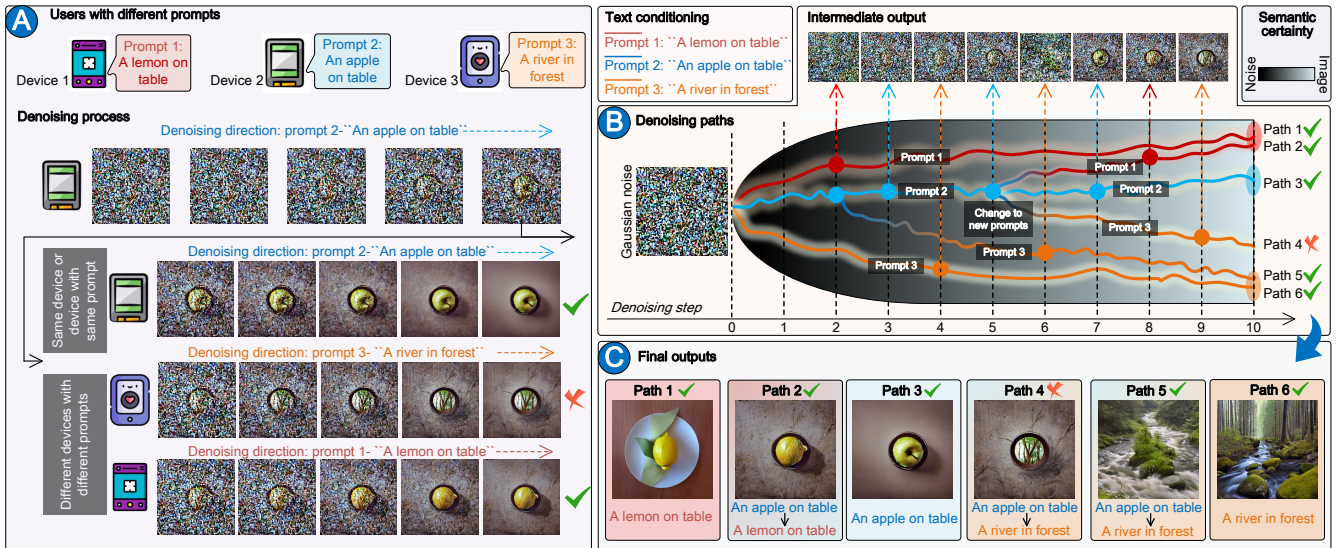
Fig. 2. The working principle of the GDM and motivations behind distributed denoising inference process. **Part A** depicts the cooperative inference process across devices where, starting with Gaussian noise on *Device 2*, it denoises using *Prompt 2* before *Devices 1* and 3 continue in succession towards their respective prompts. **Part B** shows the fundamentals of distributed GDM inference, illustrating how denoising path directions alter with changing prompts, and emphasizing the high semantic similarity of *Prompt 1* to *Prompt 2*, contrasting it with the distance between *Prompt 2* and *Prompt 3*. Consequently, Path 2 aligns with *Prompt 1*'s requirements, unlike *Path 4* with *Prompt 3*. **Part C** showcases the final generation outcomes for all five paths.

studies have adopted psychological laws to approximate users' subjective QoE [9], these methods often oversimplify, failing to address the multifaceted nature of real-world applications. Another solution is leveraging Reinforcement Learning with Human Feedback (RLHF) paradigms for *management models* training, which requires continuous QoE feedback from experts. This method is costly, ethically contentious, and challenging to execute in real-time, leading to the first research question:

C1. How to obtain human-aware subjective QoE feedback efficiently and design the communication and computing resource allocation algorithm?

Addressing *C1* requires the exploration of cutting-edge approaches, among which IAI stands out as a promising solution [6]. IAI focuses on designing AI models that learn and adapt through user interaction, progressively advancing AI models' performance and operational efficacy. This paradigm shift, from static to dynamic learning systems, equips IAI-enhanced networks with the ability to offer tailored responses and proactively adapt, marking a significant stride in personalized AI-based service managements. For AIGC services, as shown in Fig. 1, we propose Reinforcement Learning With LLM Interaction (RLLI) algorithm as one step towards IAI, incorporates Deep Reinforcement Learning (DRL) for its suitability in dynamic environments [10] and Large Language Model (LLM) for advanced knowledge understanding and generative capabilities:

- DRL regards user QoE as quantifiable rewards and circumvents complexity of mathematically modeling subjective QoE. When integrated with GAI techniques such as Generative Diffusion Model (GDM) [11] that effectively handle complex data modeling and produce high-quality samples, DRL can be further enhanced to allocate network resources efficiently while factoring in user satisfaction.

- LLM-empowered generative agents can represent real AIGC users with various personalities to generate QoE feedback, minimizing human resource input and associated ethical risks. By embedding human personality traits into generative agents through prompts [12], these generative agents can simulate human interaction in the training of DRL algorithms.

Furthermore, AIGC service models, while delivering a range of services, introduce significant energy demands during the inference phase [5]. Particularly in GDM-based image generation, a series of denoising steps are fundamental for generating high-quality images. This process requires iterative computation to reduce noise in the image, leading to increased energy and time consumption that accumulates over the sequence of denoising operations [5]. Furthermore, transmitting the generated high-quality images, crucial in real-time applications such as augmented reality and telemedicine, demands extensive network bandwidth [13], posing stringent demand for emerging sixth-generation (6G) networks with human-centric and high QoE requirements [14]. These factors constitute the second research question:

C2. How to harness network capabilities to facilitate energy-efficient and low-latency GDM inference?

Fortunately, advancements in model compression facilitate the deployment of large GAI models directly on network edge devices [15], [16]. This forms a foundation for network-assisted AIGC, particularly collaborative distributed diffusion model [17], to address *C1*. As shown in Part A of Fig. 2, by distributing the denoising steps across multiple network edge devices, we can achieve a more flexible and efficient network resource utilization. More importantly, generation tasks with semantically similar prompts can share several denoising steps, thereby saving overall energy and time consumption. As shown in Part B of Fig. 2,

the denoising *Path 2*, which starts with "*Prompt 2: An apple on table*" and switches to "*Prompt 1: A lemon on table*" can still converge nearly with *Path 1* that uses "*Prompt 1*" throughout. We can observe from Part C of Fig. 2 that when employing an appropriate distributed denoising process, such as switching prompts in an early stage or maintaining semantic similarity between prompts, high-quality images can be generated that is corresponding to user prompts while reducing overall resource consumption. For example, we can observe a clear reduction in energy and time costs when generating images via *Path 2* and *Path 3*, compared to independent operations through *Path 1* and *Path 3*.

Note that the distributed GDM-based AIGC framework introduces the semantic fusion from prompts of multiple users. Therefore, the quality of generated images is impacted by the communication and computing resources allocation scheme designed by the RLLI algorithm. Our edge-based IAI solution tackles a new optimization dimension introduced by this dependency, aiming to enhance the AIGC service and improve user QoE. The contributions of this paper are summarized as follows.

- We introduce a collaborative distributed GDM-based AIGC framework for image generation services. This approach enhances user privacy by generating the final content on edge devices, reducing the total network energy and time overheads (for *C1*).
- We present a QoE feedback scheme by using LLM-empowered generative agents to simulate the human's different personalities. With the aid of prompts and assigning one agent per user, generative agents can mimic users of diverse subjective preferences, delivering evaluations of quality of generated images (for *C2*).
- We propose an IAI algorithm, i.e., RLLI, with LLM-generated QoE at its core. The goal is to determine the optimal denoising steps, i.e., computing energy consumption, at server and user devices, and downlink transmission power, i.e., communications energy consumption, of the server to user devices, based on the user personalities and wireless conditions (for *C2*).

The rest of this paper is organized as follows: Section 2 reviews related literature. In Section 3, we describes the system model and formulates the problem for our distributed GDM-based AIGC framework. Section 4 details the RLLI algorithm. Section 5 conducts a evaluation of the proposed framework and RLLI algorithm. The paper concludes with Section 6. A list of mathematical symbols and functions most frequently used in this paper is available in Table 1.

2 RELATED WORK

In this section, we discuss several related works, including GDM, aesthetics analysis, and LLM.

2.1 Generative Diffusion Models

GDMs are fundamental techniques in various AIGC services. Applications of GDMs range from image and video generation in computer vision via DDPM [18] and video diffusion models [19], to text generation and editing through Diffusion-LM [20] and DiffusER [21], to audio synthesis with ProDiff [22] and DiffWave [23], as well as specialized

TABLE 1
Mathematical Notations

$\boldsymbol{c}_k$	The prompt from the k-th user, where $k = 1, \ldots, K$
$\mathcal{D}$	The decoder that decodes a latent representation in the latent space into an image in the RGB space
δ_0	The energy cost for each denoising step of the server
δ_k	The energy cost for each denoising step of the k-th device
E_{T}	The energy budget in the server
E_{T_k}	The energy budget in the k-th device
$\mathcal{E}$	The encoder that encodes an image in the RGB space into a latent representation in the latent space
$\boldsymbol{g}_k$	The wireless channel gains from the server to the k-th device
K	The total number of users
P_k	The transmission power from the server to the k-th device
$\mathcal{Q}_k$	The QoE of the k-th user
$\mathcal{Q}_{\mathrm{th}}$	The QoE threshold
t_0	The number of denoising steps in the server
t_k	The number of denoising steps in the k-th device
$\tau(\cdot)$	The domain-specific encoder that projects $\boldsymbol{c}$ to a latent representation
$\boldsymbol{u}_k$	The personality of the k-th user
$\boldsymbol{\varepsilon}_\theta$	The denoising network of the GDM

tasks such as graph generation [24] and molecular structure creation [25]. Increasingly, there is a demand for deploying GDMs on network edge devices for privacy-sensitive applications. Advances in model compression have enabled GDMs to operate on edge devices, yet the inference process of GDMs, i.e., executing denoising steps, is energy-intensive, adding to the overall network energy burden. Fortunately, the architecture of denoising chain opens up opportunities for novel distributed computing methods. Specifically, cooperative distributed GDM [17] allows multiple denoising chains from several devices to share some denoising steps performed in one device, reducing overall network energy consumption.

2.2 Aesthetics Analysis and Big Five Personality Traits

Traditional advancements in Image Aesthetic Assessment (IAA) have concentrated on universal aesthetic scores, overlooking the subjectivity of aesthetic appreciation from user personality difference. Recent developments, such as those integrating the Big Five personality traits into a multi-task deep learning model [26] for IAA, represent a paradigm shift. The Big Five personality traits [27], comprising openness, conscientiousness, extraversion, agreeableness, and neuroticism, form a widely recognized framework for categorizing human personality. Specifically, openness captures creativity and a willingness of users to explore new experiences; conscientiousness involves diligence and reliability; extraversion denotes sociability and assertiveness;

agreeableness reflects cooperativeness and kindness; and neuroticism is associated with emotional instability and anxiety. Integrating these traits into IAA marks a significant evolution from generic scoring to personalized evaluations, which has a potential to align AIGC models with individual psychological profiles to AIGC services more adaptive and personalized [28].

2.3 LLM-empowered Generative Agents as Evaluators

LLMs-empowered generative agents have capabilities to process and understand complex instructions in natural language, serving as a universal interface for various tasks, including evaluative [29], [30]. Specifically, the authors in [29] explore the capabilities of ChatGPT in evaluating textual content across various human-aware criteria such as quality, tone, and coherence. These evaluations provide a foundation for extending LLM functionality into other domains. Subsequently, the authors in [31] evaluate the potential of LLMs like ChatGPT in Computational Social Science (CSS), examining their ability to perform both classification and generative tasks in a zero-shot manner. It is shown that LLMs demonstrate fair agreement with humans and can augment the annotation process. More recently, the authors in [32] show that modern role-playing LLMs can successfully mimic specific personality traits, achieving an 82.8% alignment with human perceptions. In light of these capabilities, it becomes compelling to leverage LLM-empowered generative agents for simulating users with diverse subjective preferences in image evaluation tasks, proposing generative agents' feedback as a viable alternative to human feedback in training service management algorithms.

3 SYSTEM MODEL AND PROBLEM FORMULATION

In this section, we analyze the principles and conditions under which GDMs can be executed separately on different devices. Furthermore, we discuss the deployment method and formulate the user-centric QoE optimization problem in our proposed distributed GDM-based AIGC framework.

3.1 Distributed Generative Diffusion Model-based AIGC

3.1.1 Latent Diffusion Models

GDMs, as illustrated in Part A of Fig. 3, are probabilistic models constructed to capture a data distribution through a process of iteratively denoising a sample from a normal distribution, mirroring a reverse of the Markov chain process over T steps. The Stable Diffusion [4] stands out by using latent GDM, operating in the latent space rather than the high-dimensional image pixel space. Instead of manifesting a perturbed image, latent GDM introduces "latent noise", i.e., a stochastic tensor in the latent space, during training to perturb the latent image representation. For example, an image with 512×512 resolution, the corresponding latent size is a much smaller, i.e., $4 \times 64 \times 64$, enabling faster processing and less memory usage.
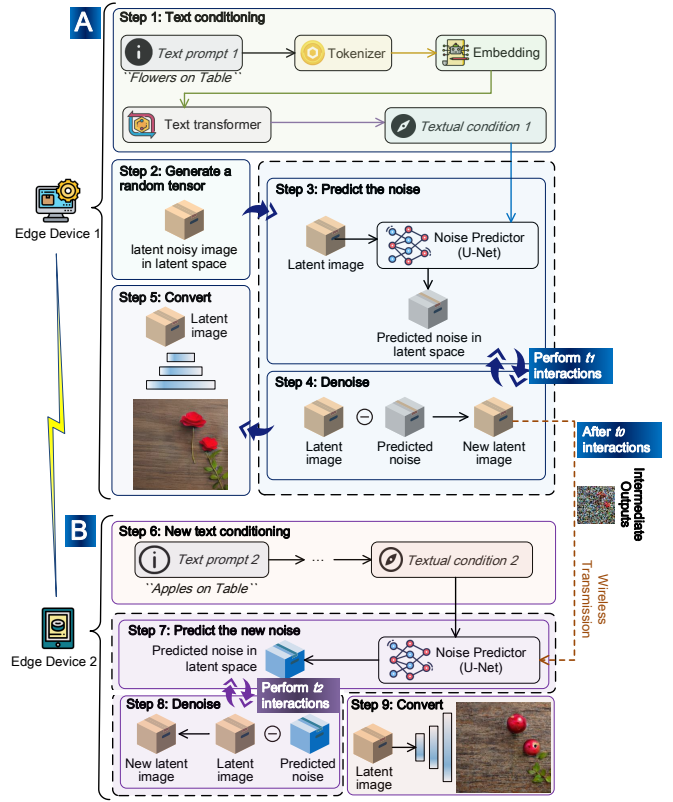

Fig. 3. The working steps of GDM-based text-to-image generation service, and the principle to achieve multi-device distributed denoising process.

Diving deeper into the mechanics, we consider $\boldsymbol{x}_0 \in R^{H \times W \times 3}$ is an image in Red, Green & Blue (RGB) space. The encoder $\mathcal{E}$ encodes $\boldsymbol{x}_0$ into a latent representation as

$$\boldsymbol{z}_0 = \mathcal{E}\left(\boldsymbol{x}_0\right), \qquad (1)$$

where $\boldsymbol{z}_0 \in R^{h \times w \times r}$. The encoder $\mathcal{E}$ downsamples the image $\boldsymbol{x}_0$ by a factor f, i.e., $f = H/h = W/w$. The decoder $\mathcal{D}$ reconstructs the image from the latent representation as

$$\tilde{\boldsymbol{x}}_0 = \mathcal{D}\left(\boldsymbol{z}_0\right) = \mathcal{D}\left(\mathcal{E}\left(\boldsymbol{x}_0\right)\right). \qquad (2)$$

GDMs can be specified in terms of a signal-to-noise ratio (SNR) as

$$\gamma\left(t\right) = \frac{\alpha_t^2}{\sigma_t^2}, \qquad (3)$$

where α_t and σ_t are strictly positive scalar-value functions of t, and $\gamma\left(t\right)$ is strictly monotonically decreasing in time, i.e., $\gamma\left(t\right) < \gamma\left(s\right)$ for any $t > s$. We consider that both α_t and σ_t are smooth, such that their derivatives with respect to t are finite [33]. This diffusion process specification includes the variance-preserving diffusion process as a special case [18], [33], where $\alpha_t = \sqrt{1 - \sigma_t^2}$. Another special case is the variance-exploding diffusion process [34], [35], where $\alpha_t^2 = 1$. We use the variance-preserving version in this paper.

By starting from a data sample $\boldsymbol{z}_0$, a forward diffusion process q can be defined as

$$q\left(\boldsymbol{z}_t | \boldsymbol{z}_0\right) = \mathcal{N}\left(\boldsymbol{z}_t | \alpha_t \boldsymbol{z}_0, \sigma_t^2 \boldsymbol{I}\right). \qquad (4)$$

The Markov structure for $t > s$ can be expressed as

$$q\left(\boldsymbol{z}_t | \boldsymbol{z}_s\right) = \mathcal{N}\left(\boldsymbol{z}_t | \alpha_{t|s}\boldsymbol{z}_0, \sigma_{t|s}^2\boldsymbol{I}\right), \qquad (5)$$

where $\alpha_{t|s} = \alpha_t/\alpha_s$ and $\sigma_{t|s}^2 = \sigma_t^2 - \alpha_{t|s}^2\sigma_s^2$.

Denoising GDMs are generative models p which revert the forward diffusion process with a similar Markov structure running backward as

$$p\left(\boldsymbol{z}_0\right) = p\left(\boldsymbol{z}_T\right)\prod_{t=1}^{T} p\left(\boldsymbol{z}_{t-1} | \boldsymbol{z}_t\right). \qquad (6)$$

The prior $p\left(\boldsymbol{z}_T\right)$ is typically choosen as a standard normal distribution. We parameterize $p\left(\boldsymbol{z}_{t-1} | \boldsymbol{z}_t\right)$ to specify it in terms of the true posterior $q\left(\boldsymbol{z}_{t-1} | \boldsymbol{z}_t, \boldsymbol{z}_0\right)$. We use the network with parameter θ, i.e., $\boldsymbol{\varepsilon}_\theta\left(\boldsymbol{z}_t, t\right)$, to estimate the unknown original data sample $\boldsymbol{z}_0$. Then, we obtain that [36]

$$\begin{aligned} p\left(\boldsymbol{z}_{t-1} | \boldsymbol{z}_t\right) &= q\left(\boldsymbol{z}_{t-1} | \boldsymbol{z}_t, \boldsymbol{z}_0\right) \\ &= q\left(\boldsymbol{z}_{t-1} | \boldsymbol{z}_t, \boldsymbol{z}_\theta\left(\boldsymbol{z}_t, t\right)\right) \\ &= \mathcal{N}\left(\boldsymbol{z}_{t-1} | \mu_\theta\left(\boldsymbol{z}_t, t\right), \sigma_{t|t-1}^2\frac{\sigma_{t-1}^2}{\sigma_t^2}\boldsymbol{I}\right), \end{aligned} \qquad (7)$$

where

$$\mu_\theta\left(\boldsymbol{z}_t, t\right) = \frac{\alpha_{t|t-1}\sigma_{t-1}^2}{\sigma_t^2}\boldsymbol{z}_t + \frac{\alpha_{t-1}\sigma_{t|t-1}^2}{\sigma_t^2}\boldsymbol{\varepsilon}_\theta\left(\boldsymbol{z}_t, t\right). \qquad (8)$$

We use the reparameterization [18]

$$\boldsymbol{\varepsilon}_\theta\left(\boldsymbol{z}_t, t\right) = \frac{\boldsymbol{z}_t - \alpha_t\boldsymbol{z}_\theta\left(\boldsymbol{\varepsilon}_t, t\right)}{\sigma_t}, \qquad (9)$$

to express the reconstruction term as a denoising objective.

For convenience, we denote the denoising process that involves (7), (8), and (9) as $Denoise\left(\cdot\right)$

$$\boldsymbol{z}_{t-1} = Denoise\left(\boldsymbol{z}_t, t\right). \qquad (10)$$

The corresponding loss function to train the latent GDM can be simplified to

$$\mathcal{L}_{GDM} = E_{\boldsymbol{z}, \varepsilon \sim \mathcal{N}(0,1), t}\left[\|\varepsilon - \boldsymbol{\varepsilon}_\theta\left(\boldsymbol{z}_t, t\right)\|_2^2\right], \qquad (11)$$

with t uniformly sampled from $\{1, \ldots, T\}$. The neural backbone is realized as a time-conditional UNet [37]. Since the forward process is fixed, $\boldsymbol{z}_t$ can be efficiently obtained from $\mathcal{E}$ during training, and samples from $p\left(z\right)$ can be decoded to image space with a single pass through $\mathcal{D}$.

3.1.2 Conditioning Mechanisms

Similar to other types of generative models [38], [39], GDMs are capable of modeling conditional distributions. This can be implemented with a conditional denoising auto-encoder $\boldsymbol{\varepsilon}_\theta\left(\boldsymbol{z}_t, t, \boldsymbol{c}\right)$ to control the synthesis process through inputs $\boldsymbol{c}$ such as text [40], semantic maps [41] or other image-to-image translation tasks [42]. To pre-process $\boldsymbol{c}$ from various modalities, such as language prompts, a domain-specific encoder is introduced that projects $\boldsymbol{c}$ to a latent representation $\tau\left(\boldsymbol{c}\right)$. Based on image-conditioning pairs, we then train the conditional latent GDM via

$$\mathcal{L}_{LDM} = E_{\boldsymbol{z}, \varepsilon \sim \mathcal{N}(0,1), t, \boldsymbol{c}}\left[\|\varepsilon - \boldsymbol{\varepsilon}_\theta\left(\boldsymbol{z}_t, t, \tau\left(\boldsymbol{c}\right)\right)\|_2^2\right]. \qquad (12)$$

In the inference process, the denoising functions can be updated accordingly, by adding $\boldsymbol{c}$ as the condition together

---

Algorithm 1 Distributed latent GDM Inference Process Among K Devices

Input: the textual prompt $\{\boldsymbol{c}_1, \ldots, \boldsymbol{c}_K\}$ from devices $1, \ldots, K$, respectively
Output: Generated image $\tilde{\boldsymbol{x}}_0$ for any device k $(k = 2, \ldots, K)$
1: ## In Device 1
2: Sample initial Gaussian noise $\boldsymbol{z}_T$ in the latent space
3: **for** $t = T$ to $t_{\text{off}} + 1$ **do**
4: $\quad \boldsymbol{z}_{t-1} \leftarrow \text{Denoise}(\boldsymbol{z}_t, t, \tau\left(\boldsymbol{c}_i\right))$, i.e., (13)
5: **end for**
6: ## Wireless Transmission
7: Transmit the $\boldsymbol{z}_{t_{\text{off}}}$ from device 1 to devices $2, \ldots, K$
8: ## In Device k $(k = 2, \ldots, K)$
9: **for** $t = t_{\text{off}}$ to 1 **do**
10: $\quad \boldsymbol{z}_{t-1} \leftarrow \text{Denoise}(\boldsymbol{z}_t, t, \tau\left(\boldsymbol{c}_k\right))$, i.e., (13)
11: **end for**
12: ## Image Reconstruction
13: $\tilde{\boldsymbol{x}}_0 \leftarrow \mathcal{D}(\boldsymbol{z}_0)$
14: **return** $\tilde{\boldsymbol{x}}_0$

---

with step information t as

$$\boldsymbol{z}_{t-1} = Denoise\left(\boldsymbol{z}_t, t, \tau\left(\boldsymbol{c}\right)\right). \qquad (13)$$

3.1.3 Distributed Diffusion Model Inference

The distributed GDM inference process relies on sequential denoising guided by textual prompts. We analyze mathematically the conditions for changing textual prompts while still ensure that the denoising results remain effective and reliable. Specifically, we consider the latent space, in which the diffusion process takes place, to be the Euclidean space denoted as $\mathcal{L}$. Every point in $\mathcal{L}$ corresponds to a latent vector. The analysis includes the following steps:

1) *Defining Denoising Path and Semantic Distance*:
   For each textual prompt $\boldsymbol{c}$, the denoising path, evolving from the initial Gaussian noise to the targeted semantic representation, is represented by $P_{\boldsymbol{c}} : [T, 0] \rightarrow \mathcal{L}$. Here, $P_{\boldsymbol{c}}\left(T\right)$ represents the Gaussian noise point, i.e., the start point in Part B of Fig. 2, while $P_{\boldsymbol{c}}\left(0\right)$ corresponds to the latent representation of the final generated image under the prompt $\boldsymbol{c}$, i.e., the end point in Part B of Fig. 2.
   The semantic distance between two prompts, $\boldsymbol{c}_i$ and $\boldsymbol{c}_j$, in the latent space is defined by the Euclidean distance between their respective denoising path endpoints as

$$d\left(\boldsymbol{c}_i, 0, \boldsymbol{c}_j, 0\right) = \|P_{\boldsymbol{c}_i}\left(0\right) - P_{\boldsymbol{c}_j}\left(0\right)\|. \qquad (14)$$

   The semantic distance provides a direct measure: if the semantic information of $\boldsymbol{c}_i$ and $\boldsymbol{c}_j$ are closely related, their corresponding semantic representations, i.e., latent vectors, and the denoising paths under their guidance, should also be proximate in $\mathcal{L}$. Consequently, a smaller $d\left(\boldsymbol{c}_i, 0, \boldsymbol{c}_j, 0\right)$ indicates that substituting $\boldsymbol{c}_i$ for $\boldsymbol{c}_j$ is less likely to degrade the quality of generated images.

2) *Semantic Analysis:*
   Another key observation is that extending the denoising path, i.e., $P_{\boldsymbol{c}}\left(t\right)$ with t from T to 0, progressively incorporates the semantic information of the textual prompt $\boldsymbol{c}$ into the path. To measure the difference in semantic information encoded within the latent vectors at step t

between prompts $\boldsymbol{c}_i$ and $\boldsymbol{c}_j$, we employ the Kullback-Leibler (KL) divergence:

$$\mathcal{K}\left(p\left(\boldsymbol{z}_t|\boldsymbol{c}_i\right)||p\left(\boldsymbol{z}_t|\boldsymbol{c}_j\right)\right) = \sum_{z \in \boldsymbol{z}_t} p\left(z|\boldsymbol{c}_i\right) \log \frac{p\left(z|\boldsymbol{c}_i\right)}{p\left(z|\boldsymbol{c}_j\right)}. \quad (15)$$

At the beginning of the denoising process, i.e., $t = T$, the noise component dominates, leading to a latent space with high entropy due to the absence of any meaningful semantic information. Thus, both prompts would produce almost similar distributions for the latent vectors. As a result, the KL divergence, $\mathcal{K}$, would be small, suggesting minimal difference between the paths $P_{\boldsymbol{c}_i}$ and $P_{\boldsymbol{c}_j}$, which means that $d\left(\boldsymbol{c}_i, T, \boldsymbol{c}_j, T\right)$ is small for any $\boldsymbol{c}_i$ and $\boldsymbol{c}_j$. With the progression of denoising, the influence of the prompts begins to introduce semantic information, leading to a reduction in entropy.

3) *Switching Denoising Path*: Assuming a denoising path have been progressed t_{off} steps under $\boldsymbol{c}_i$ to an intermediate point $P_{\boldsymbol{c}_i}(t_{\text{off}})$, where $0 < t_{\text{off}} < T$. Now, the flowing denoising path should cover the semantic distance:

$$d\left(\boldsymbol{c}_i, t_{\text{off}}, \boldsymbol{c}_i, 0\right) = \|P_{\boldsymbol{c}_i}(t_{\text{off}}) - P_{\boldsymbol{c}_i}(0)\|. \quad (16)$$

However, if we intend to switch the prompt from $\boldsymbol{c}_i$ to $\boldsymbol{c}_j$, the distance from $P_{\boldsymbol{c}_i}(t_{\text{off}})$ to the end-point of $\boldsymbol{c}_j$ is:

$$d\left(\boldsymbol{c}_i, t_{\text{off}}, \boldsymbol{c}_j, 0\right) = \|P_{\boldsymbol{c}_i}(t_{\text{off}}) - P_{\boldsymbol{c}_j}(0)\|. \quad (17)$$

This distance $d\left(\boldsymbol{c}_i, t_{\text{off}}, \boldsymbol{c}_j, 0\right)$ is crucial as it informs the extent of path correction needed to align the denoising process towards the semantics of $\boldsymbol{c}_j$. From the above analysis, we conclude the following conditions for our distributed GDM-based AIGC framework:

- The new prompt $\boldsymbol{c}_j$ should have close semantic information related to $\boldsymbol{c}_i$, reducing the difference between (16) and (17).
- The transition to $\boldsymbol{c}_j$ should be made in a relatively early stage of the denoising process, i.e., when $\mathcal{K}$ as given in (15) is small, to reduce the influence of $\boldsymbol{c}_i$ and allowing $\boldsymbol{c}_j$ to predominantly lead the denoising direction.

4) *Image Reconstruction*: The image $\tilde{\boldsymbol{x}}_0$ reconstructed from the latent representation $P_{c_j}(0)$ reflects the semantic influence of $\boldsymbol{c}_j$:

$$\tilde{\boldsymbol{x}}_0 \approx \mathcal{D}\left(P_{\boldsymbol{c}_j}(0)\right). \quad (18)$$

The decoder $\mathcal{D}$ maps the latent representation back to the image space. A high quality in $\tilde{\boldsymbol{x}}_0$ means the generated image is a precise representation, effectively capturing the semantics associated with $\boldsymbol{c}_j$.

The overall algorithm for distributed latent GDM inference process among K devices is given as **Algorithm** 1. Note the our framework efficiently supports not only synchronous but also asynchronous operations, using a simple caching mechanism as discussed in Section 6.

3.2 Deployment Method

The proposed distributed GDM-based AIGC framework relies on the flexibility of the denoising path. By sharing intermediate denoised results among network devices, the overall energy consumption of the system is reduced. Three
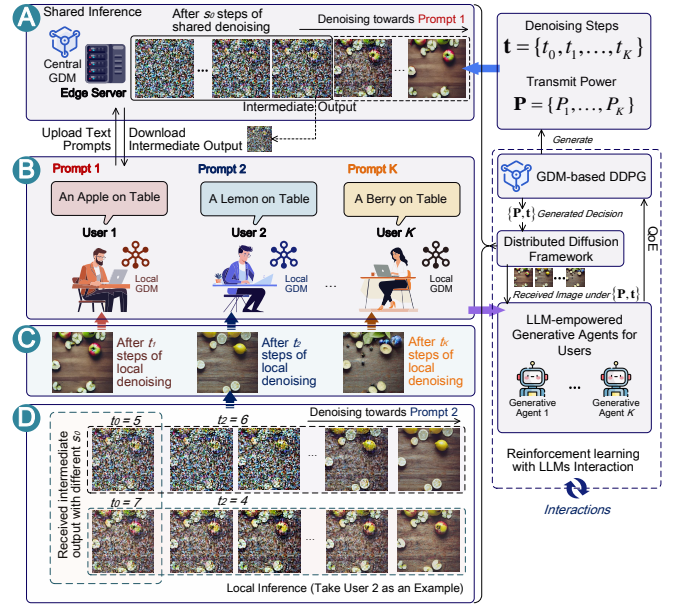

Fig. 4. Deployment method for distributed GDM-based text-to-image AIGC services: **Part A** illustrates the Shared Inference mechanism where users with semantically similar prompts collaborate with the server that executes shared denoising steps. **Part B** highlights the diverse text-to-image requirements of each of the K concurrent users. Following initial server processing, **Part D** delves into the distributed denoising process by each individual user. **Part C** presents the final generated images corresponding to user-specific prompts.

key network architectures are considered as the deployment methods:

1) The *Edge-to-Multiple Devices* architecture executes shared denoising steps at an edge server, and then transmitting intermediate denoised results to the user devices, as shown in Fig. 4.
2) The *Device-to-Device* approach fosters a partnership between two devices, jointly executing denoising tasks, optimizing energy usage, and safeguarding user privacy, as shown in Fig. 3.
3) The strategy of *Forming a Cluster among Multiple Devices*, either with the assistance of an edge server or through self-organization, bolsters system adaptability and scalability to local requirements and environments, as shown in Part A of Fig. 2.

Without loss of generality, we focus on the *Edge-to-Multiple Devices* architecture for the distributed GDM-based AIGC framework. Our analytical approach can be extended easily to two other architectures. Here, we consider a server executes t_0 denoising steps, followed by K users with each executing t_k steps. Each denoising step at the server incurs an energy cost δ_0, while every user device has its corresponding unit energy cost δ_k. Additionally, to transmit intermediate denoised results to the k-th user, the server utilizes transmission power P_k with unit energy cost β.

The QoE values are affected by communication and computing resource allocation scheme and, especially, user's personality, $\boldsymbol{u}_k$. This personality dictates the aesthetic preferences to a given image, resulting in subjective QoE values. Here, our resource allocation variables for communication

and computing are delineated as

$$\boldsymbol{t} = \{t_0, t_1, \ldots, t_K\}, \tag{19}$$

and

$$\boldsymbol{P} = \{P_1, \ldots, P_K\}. \tag{20}$$

The resource allocation variables, $\boldsymbol{t}$ and $\boldsymbol{P}$, are significant in determining the efficacy of the AIGC service:

- The transmission power, $\boldsymbol{P}$, impacts the bit error probability (BEP) during wireless transmission. Lower power levels risk degrading the integrity of the transmitted intermediate denoised results, potentially diminishing the quality of generated images.
- The number of denoising steps, $\boldsymbol{t}$, directly affects the quality of generated images. More steps allow for a finer degree of control and correction, which results in higher image fidelity [5].
- Notably, when transmission power is insufficient, which increases the bit errors in intermediate denoised results, adding more denoising steps can improve the final image quality [17]. These additional steps function as an error-correction phase, reducing inaccuracies and improving the final result.

3.3 User-centric QoE Maximization Problem

The central challenge is maximizing the sum subjective QoE across all users, while considering the user personalities, objective wireless conditions, energy constraints, and QoE threshold. Mathematically, our objective and constraints can be expressed as

$$\max_{\{\boldsymbol{t}, \boldsymbol{P}\}} \quad \sum_{k=1}^{K} \mathcal{Q}_k(t_0, t_k, P_k, \boldsymbol{u}_k), \tag{21}$$

$$s.t., \quad \delta_k t_k \leq E_{\mathrm{T}_k}, \quad \forall k \in \{1, \ldots, K\} \tag{22}$$

$$\mathcal{Q}_k(t_0, t_k, P_k, \boldsymbol{u}_k) \geq \mathcal{Q}_{\mathrm{th}}, \quad \forall k \in \{1, \ldots, K\} \tag{23}$$

$$\delta_0 t_0 + \beta \sum_{k=1}^{K} P_k \leq E_{\mathrm{T}}. \tag{24}$$

The first constraint captures the computing energy limitations of edge devices for executing denoising steps. The second constraint shows that the AIGC service should meet users' minimum QoE requirements. The third constraint, the most critical, highlights energy limitations and necessitates a trade-off between communication and computing resources. Specifically, higher transmission power lowers BEP and improves the accuracy of transmitted intermediate denoised results. However, excessive transmission power limits the available energy for denoising steps, directly affecting the final image quality. Furthermore, if the transmission power is inadequate, even improved denoising steps at the edge device cannot compensate for the bit errors in received intermediate denoised results.

In the following, we use the RLLI method for the user-centric QoE maximization problem in our proposed distributed GDM-based AIGC framework.

4 REINFORCEMENT LEARNING WITH LLMS FEEDBACK

In this section, we propose the RLLI method. Specifically, we first discuss aesthetic-aware QoE modeling, and then we explain how to use the LLM-empowered generative agents as evaluators to feedback their subjective QoE values as the reward for DRL algorithms.

4.1 Aesthetic-aware QoE Modeling

4.1.1 Big Five Personality Traits

Incorporating generative agents into the DRL training process allows for the meaningful integration of human subjective factors, specifically aesthetic preferences, a critical component affecting QoE in image-related AIGC services. Research has shown that aesthetic preferences can be influenced by an individual's personality traits [26]–[28]. The Big Five personality traits [27], also known as the Five-Factor Model (FFM), is a widely accepted framework for understanding individual differences in personality[1]. The Big Five model consists of five broad dimensions of personality traits including

- *Openness:* A trait characterized by a deep affinity for imagination, novel experiences, and a broad spectrum of interests.
- *Conscientiousness:* Denotes meticulousness and structure, often manifesting in methodical, goal-oriented behaviors.
- *Extraversion:* Embodies individuals who thrive in social interactions, drawing energy from a company of others.
- *Agreeableness:* Reflects proclivities towards trustworthiness, altruism, and prosocial behaviors.
- *Neuroticism:* Typified by emotional fluctuations and heightened sensitivity to environmental stressors and adversities.

Each of these traits represents a continuous spectrum of personality characteristics. Considering that recent study has demonstrated that LLMs can effectively simulate the Big Five personality traits and achieve an 82.8% alignment with human perceptions of these characteristics [32], we use the Big Five personality model as the basis for enabling LLM-empowered generative agents to mimic AIGC service users' personalities [12].

In Fig. 5, we display five exemplary user profiles from the PsychoFlickr dataset [28], i.e., their Big Five personality scores and selected favored images. These profiles provide empirical evidence for the relationship between individual personality traits and aesthetic preferences in image selection. Turning to the issue of shared denoising, unlike individual denoising processes, the presence of multiple prompts sharing shared denoising steps results in interrelated final images, as we discussed in Section 3.1.3. Specifically, the more shared steps among prompts, the greater the mutual influence on the generated images. This is critical from the user QoE perspective, particularly for those with distinct personality traits. For instance, as depicted in Part B of Fig. 6, one user, scoring high in agreeableness, might prefer an image generated from the prompt *"A dog sits in front of a bush"* that has a well-groomed dog. However, if this prompt shares several shared denoising steps with another prompt such as *A tiger sits in front of a bush"*, the final generated images for this user may have a dog that

---

1. One example of open source Big Five personality traits tests: https://bigfive-test.com.
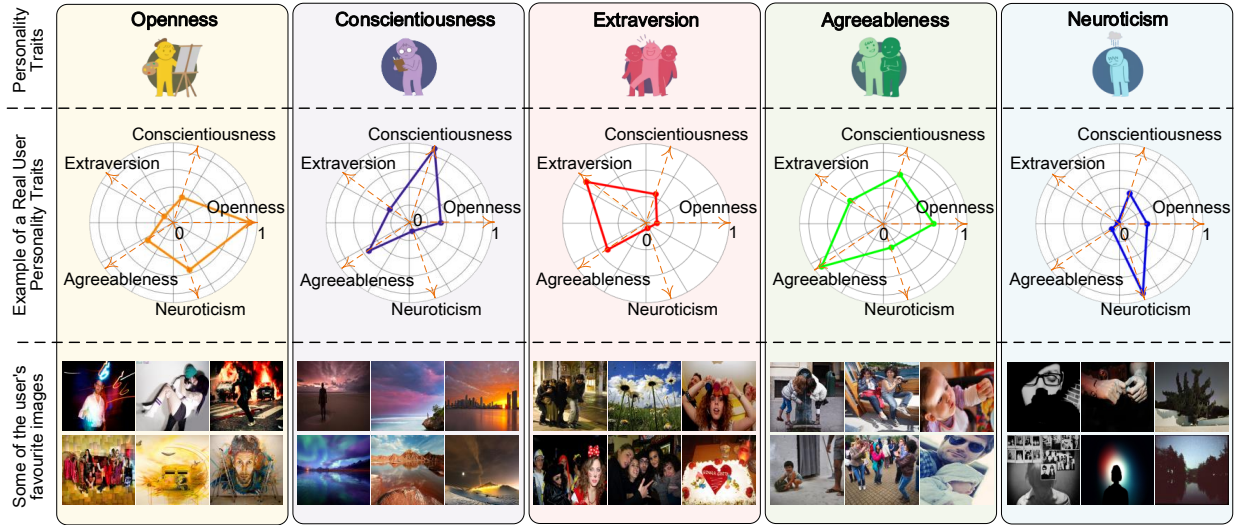
Fig. 5. Five types of personality traits in the Big-Five personality model: Openness, Conscientiousness, Extraversion, Agreeableness, and Neuroticism. We show real user personality scores from the PsychoFlickr database, along with examples of the images that they prefer.

exhibits stylistic features of a tiger, causing the low QoE. Thus, the settings for shared denoising steps are pivotal in achieving maximum sum QoE.

4.1.2 Prompt Design for LLM-empowered Generative Agents

The LLM-empowered generative agents present a powerful mechanism to feedback human-aware subjective QoE values for the generated content. A critical aspect is the initial prompts that guide the generative agents' subjective QoE assessment [12]. The initial prompts setting process is illustrated in Parts A and C of Fig. 6, including general setup and GA-specific settings:

- In the general setup stage, the Big-Five personality traits are introduced to all K generative agents to enhance their understanding and responsiveness to these traits.
- In the GA-specific settings stage, the users' Big-Five personality traits are individually configured for generative agents, enabling generative agents' similar subjective assessments to given images as real users.

With the Big-Five model, the personality of the k-th user, i.e., $\boldsymbol{u}_k$, can be expressed as

$$\boldsymbol{u}_k = [o_k, c_k, e_k, a_k, n_k], \tag{25}$$

where $k = 1, \ldots, K$, and each element in $\boldsymbol{u}_k$ corresponds to a score in one of the Big Five personality traits. Note that the vector $\boldsymbol{u}_k$ is significant in our RLLI framework in tailoring the subjective QoE assessment according to individual preferences. Specifically, $\boldsymbol{u}_k$ serves as the *personality traits tuning* for generative agents. Furthermore, $\boldsymbol{u}_k$ acts as the user identifier that can be used for the DRL-based resource allocation algorithm design, similar to user representation in AI-based recommendation systems where user preferences are captured and embedded to provide personalized recommendations [43].

4.2 Reinforcement Learning With LLMs Feedback Framework

LLMs are typically designed for language tasks, yet their ability to interpret various task instructions articulated in language has shown promise for acting as universal interfaces for general-purpose assistants [15], [31]. For our proposed RLLI framework, to leverage the inferential capabilities of LLM to simulate users with different personality traits, the LLM-empowered generative agents' instructional capacity has to be extended to encompass visual domains.

4.2.1 Visual Instruction Tuning (VIT)

The VIT framework elevates the instruction tuning paradigm into the multi-modal sphere, leveraging LLMs to process both textual and visual information [44]. With the demonstrated proficiency of LLMs such as ChatGPT and GPT4[2] in executing complex instructions, we has seen the rise of accessible open-source LLMs like LLaMA [45], further simplifying the adoption of VIT.

Specifically, VIT processes an image input to extract features that are then converted into language embedding tokens using a trainable projection matrix [44]. Training involves generating multi-turn conversational sequences from each image to form instructions and predict answer tokens using an auto-regressive objective. The model undergoes a two-stage instruction tuning: initially, it aligns features using image-text pairs to train the visual tokenizer while keeping LLM and visual encoder weights static. Subsequently, it fine-tunes both the projection matrix and LLM weights using varied datasets to improve response diversity. After VIT, an image can be processed by the LLM-powered generative agents. This advancement extends the GA's capabilities beyond merely handling text and allows for the subjective evaluation of the image's quality.

Thus, in this paper, we use the LLaMA-based LLaVA [44], i.e., an end-to-end trained large multi-modal

---

2. Although the current GPT4 has image reading capabilities, it remains a proprietary model.

A | Initial Setting of LLM-empowered Generative Agents by Prompt Engineering

Please simulate a human user with your own personality, specifically aligned with the **Big-Five personality traits.** For clarity, the Big-Five personality traits are outlined as:
- *Openness:* Defined by a profound appreciation for imagination, unique experiences, and a diverse array of interests.
- *Conscientiousness:* Characterized by meticulousness and systematic behaviors, particularly evident in goal-driven activities.
- *Extraversion:* Represents individuals invigorated by social engagements, garnering energy from interpersonal interactions.
- *Agreeableness:* Indicates tendencies towards trust, altruism, and collaborative behaviors.
- *Neuroticism:* Highlighted by emotional volatility and an acute awareness of external stressors and challenges.

Afterwards, I will provide you with specific personality traits setting to guide your subjective assessment of my provided image.

Prompt engineer

Certainly! I'll provide a human-like response by incorporating the Big-Five personality traits you specify. Once you share the personality traits and the image in question, I'll give you my subjective assessment.

Agent

B | An Example of the Effect of Different Combinations of Denoising Steps on the Generated Image

Prompt 1: ``A *tiger* sits in front of a bush``

Edge server → Intermediate Output → Wireless Transmission

Prompt 2: ``A *dog* sits in front of a bush``

Local GDM

Denoising steps in the user device: 8

Denoising steps in the server: *Semantic features of ``Tiger`` are enhanced.*

3 — IMAGE 1
4 — IMAGE 2
5 — IMAGE 3

Final generated image on the user device

C | Generative agents simulate users of different personalities

Embody a user characterized by the following Big Five personality traits scores:
Openness: 0.1, Conscientiousness: 0.8, Extraversion: 0.7, Agreeableness: 0.8, and *Neuroticism: 0.1*
Based on these traits, provide your aesthetic rating (ranging from 0 to 1) for the given **IMAGE 1**.

Prompt engineer

User 1

The dog on the wooden surface offers clear focus, appealing to my conscientiousness. I value the detailed features but find the blurred forest backdrop mundane due to my low openness. A clearer or intentional background would've been better. I favor simpler, recognizable scenes.
Aesthetic Rating for **IMAGE 1: 0.89**

Agent 1

Provide your aesthetic rating (ranging from 0 to 1) for the given **IMAGE 3**.

Prompt engineer

The dog that looks somewhat fierce seems out of place to my low openness. My high conscientiousness questions its safety. While the dark background is striking, the image's unusual elements feel less relevant. I seek clarity and logic in images.
Aesthetic Rating for **IMAGE 2: 0.70**

Agent 1

D | Generative agents simulate users of different personalities

Embody a user characterized by the following Big Five personality traits scores:
Openness: 0.9, Conscientiousness: 0.2, Extraversion: 0.1, Agreeableness: 0.1, and *Neuroticism: 0.8*
Based on these traits, provide your aesthetic rating (ranging from 0 to 1) for the given **IMAGE 1**.

Prompt engineer

User 2

The dog in its natural setting with a dream-like forest appeals to my high openness. However, the focus on the dog's eyes and its position on a table make me uncomfortable. Despite this, the image's simplicity intrigues me.
Aesthetic Rating for **IMAGE 1: 0.78**

Agent 2

Provide your aesthetic rating (ranging from 0 to 1) for the given **IMAGE 3**.

Prompt engineer

The dog with stripes in a field surrounded by deep-colored shrubs captures my high openness. However, my low agreeableness and conscientiousness find the combination perplexing. I'm left wondering about the peculiarity: Why does the dog also have tiger stripes?
Aesthetic Rating for **IMAGE 2: 0.83**

Agent 2

Note that the agents' response in this figure is our actual recorded result. However, in real experiments, we add the prompt ``Please only response your rating score'' to speed up the experiment and simplify the extraction of score number.
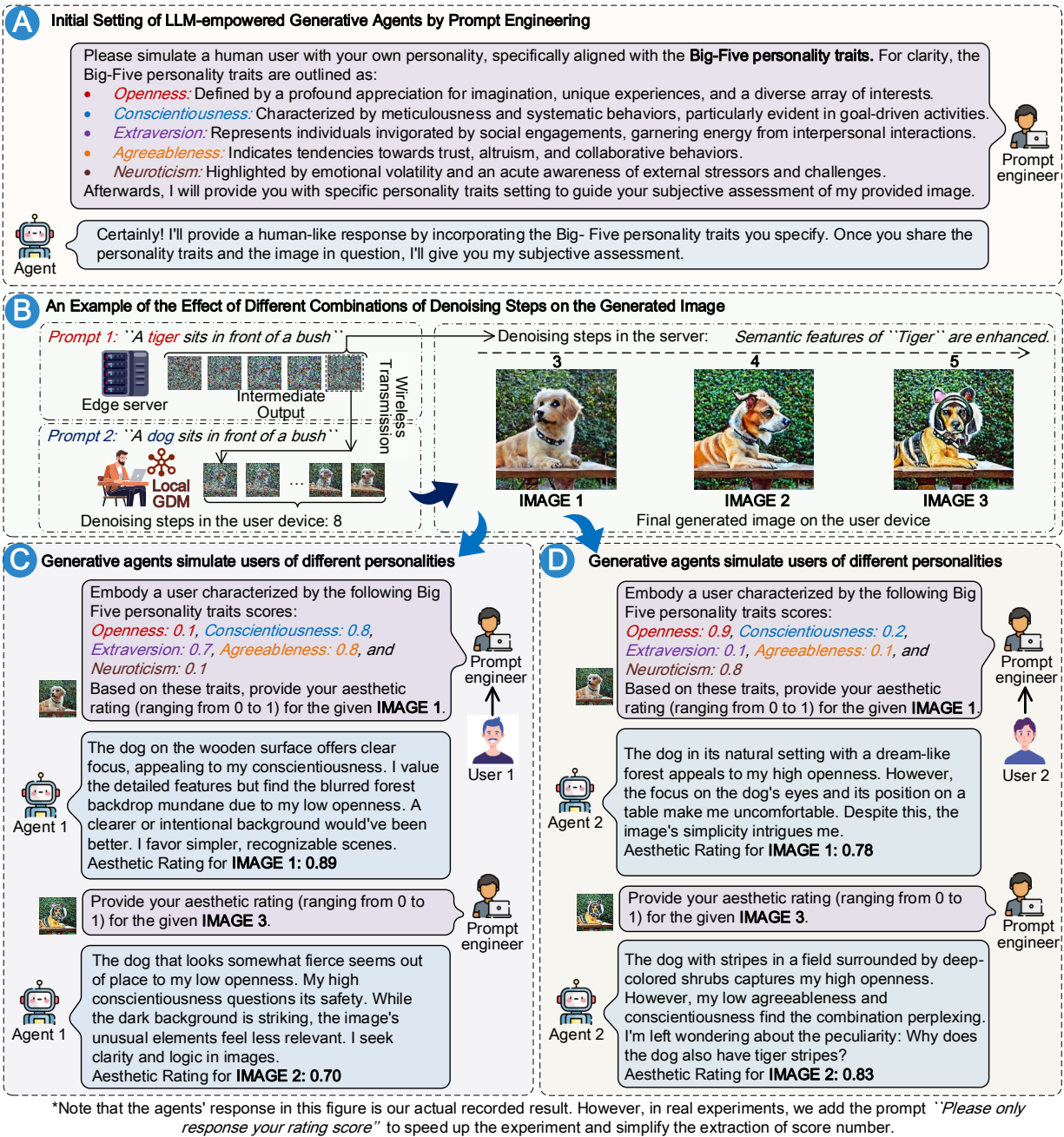
Fig. 6. Prompts for LLM-empowered generative agents settings. **Part A** illustrates the initial setup to acquaint the generative agents with the Big-Five personality traits, preparing them for the subjective assessment task. **Part B** demonstrates a case where the different numbers of shared denoising steps lead to stylistic differences in the final generated images. **Part C** and **Part D** present two user personality trait configurations and the corresponding evaluated scores of generated images. Note that the *prompt engineer* is a component of our proposed RLLI, which does not require human involvement and merely acquires the personality traits of the target user for the initial setting.

model, to empower generative agents for our RLLI algorithm. Note that RLLI's effectiveness is not confined to a specific LLM. Due to the generalizable nature of LLMs in understanding and generating language prompts [12], [45], our method remains applicable and effective across a range of LLMs, ensuring broad adaptability and relevance [3].

3. Using specialized LLMs according to specific application scenarios is expected to further enhance the performance of RLLI, which is left for our future work.

4.2.2 Reinforcement Learning with LLMs Interaction Framework

RL trains agents to maximize a reward function through interaction with an environment. Reinforcement Learning with Human Feedback (RLHF) enhances this process by introducing human insights into the policy optimization, often through demonstrations or comparative feedback [46], significantly improving conversational agents like ChatGPT. Nonetheless, both RL and RLHF encounter important challenges:

Algorithm 2 Reinforcement Learning with Large Language Model Interaction (RLLI)

Initialize: The management model with parameters $\boldsymbol{\xi}$, LLM-empowered generative agents $\boldsymbol{K}$ to simulate K users
Output: The trained management model $\boldsymbol{\xi}$

1: Input prompts to K generative agents, letting them to simulate users with different personalities
2: **for** each episode $e = 1, 2, \ldots, E$ **do**
3:      **Initialize** state $\boldsymbol{s}$
4:      **while** $\boldsymbol{s}$ is not terminal **do**
5:          Generate action $\boldsymbol{a}$ using policy $\pi_{\boldsymbol{\xi}}(\boldsymbol{s})$
6:          Obtain reward $r = \sum\limits_{k=1}^{K} \text{Agent}_k(\boldsymbol{s}, \boldsymbol{a})$
7:          Transition to new state $\boldsymbol{s}'$
8:          Store transition $(\boldsymbol{s}, \boldsymbol{a}, r, \boldsymbol{s}')$ in *Replay Buffer*
9:          Sample a random minibatch of transitions from *Replay Buffer*
10:         Update policy parameters $\boldsymbol{\xi}$
11:         $\boldsymbol{s} \leftarrow \boldsymbol{s}'$
12:      **end while**
13: **end for**

- **Real-Time Constraint.** Delayed feedback in RLHF hinder its applicability in scenarios demanding immediate response. Moreover, the continuous need for human expertise input raises costs.
- **Expert Availability.** Consistent expert interaction is challenging, inconsistent, and thus unreliable. Furthermore, the varying quality of human feedback affects the management model training.
- **Ethical and Privacy Risk.** Human-in-the-loop interaction system may present data confidentiality concerns in sensitive applications. For example, some AI-generated images are inappropriate for humans in all ages to view.

To address these challenges, we introduce RLLI, where real users can leverage LLM-empowered generative agents to provide feedback for DRL model training. These generative agents mimic users with varied personalities and provide immediate, context-aware feedback in the form of subjective QoE rewards. Consequently, RLLI offers a real-time, scalable, and financially efficient solution, mitigating the inherent constraints of RL and RLHF. The general algorithm for implementing RLLI is shown as **Algorithm** 2. Specifically, the management model initializes with parameters $\boldsymbol{\xi}$, while K LLM-empowered generative agents simulate diverse user feedback. Each episode e begins with state $\boldsymbol{s}$ and iterates until a terminal state is reached. Here, a terminal state is the endpoint of an episode, indicating task completion, step limit reached, or a failure event. Actions $\boldsymbol{a}$ are generated via policy $\pi_{\boldsymbol{\xi}}(\boldsymbol{s})$, with rewards aggregated from the agents' subjective QoE assessments. State transitions and experiences are stored in a Replay Buffer, facilitating policy parameter updates through experience replay. This iterative process, across E episodes, refines the model's decision-making capabilities by integrating feedback from generated agents interaction, culminating in a robustly trained management model.

4.3 GDM-based DDPG With LLMs Interaction for Joint Resource Allocation

DRL provides a compelling solution for solving resource allocation problems, given its capacity to learn optimal policies from high-dimensional state and action spaces [10]. Within the realm of DRL, DDPG stands out for its effectiveness in handling continuous action spaces, attributed to its utilization of an actor-critic architecture that facilitates stable learning [10], [47]. In our problem (21), the action space comprises both continuous and discrete variables, culminating in a hybrid action space [48]. To navigate this complexity, one could manipulate the continuous action space to select discrete actions [48], [49], e.g., by generating a 10-dimensional action vector with values ranging between 0 and 1, and subsequently choosing the action corresponding to the position of the maximum value. This methodology is plausible due to the continuous relaxation of discrete action spaces, allowing gradient-based optimization methods, like DDPG, to operate. By doing so, we aim to effectively handle high-dimensional hybrid action spaces, thus improving learning accuracy and efficiency. We incorporate a DDPG architecture, integrated with a GDM for the actor network. Additionally, we embed fixed Q-targets strategy to mitigate the risk of destabilized Q-values updating [50]. In the following, we explain the action, state, reward, and network training functions of our G-DDPG with LLMs interaction algorithm respectively.

Actions. The action is defined as $\boldsymbol{a}$, which includes the communication and computing resources variables, denoted as $\boldsymbol{a} = \{\boldsymbol{P}, \boldsymbol{t}\}$, where $\boldsymbol{P}$ and $\boldsymbol{t}$ are given as (19) and (20), respectively. We employ a GDM to generate an optimal communication and computing resource allocation scheme [11], as depicted in Fig. 7 and formalized in (7). The GDM-based method is distinct from the conventional back-propagation or direct optimization approaches typically employed in DRL, offering a progressive refinement of the action distribution. The action dimensionality, in a scenario where a server caters to K users, is $K + T_{\text{s}} + K T_{\text{e}}$. Here, T_{s} and T_{e} represent the maximum number of denoising steps that can be executed by the edge server and user device, respectively, under the energy constraints.

States. The state vector $\boldsymbol{s}$ encapsulates variables impacting the optimal communication and computing resource allocation scheme. Thus, $\boldsymbol{s}$ can be used as the condition in the denoising process, which can be formulated as:

$$\boldsymbol{s} = \left\{ \begin{matrix} \boldsymbol{u}_1, \ldots, \boldsymbol{u}_K, \tau(\boldsymbol{c}_1), \ldots, \tau(\boldsymbol{c}_K), \delta_0, \ldots, \delta_K, \\ \boldsymbol{g}_1, \ldots, \boldsymbol{g}_K, \mathcal{Q}_{\text{th}} \end{matrix} \right\}, \quad (26)$$

where $\boldsymbol{g}_k$ $(k = 1, \ldots, K)$ is the wireless channel gains from the server to the k-th device.

Reward. In designing the reward function for our G-DDPG model, we consider the primary objective of maximizing the sum QoE, i.e., $\sum_{k=1}^{K} \mathcal{Q}_k$, subject to energy constraints, as shown in (21). Instead of imposing hard constraints that could lead to sparse rewards and hinder the learning process, we integrate a soft constraint approach into the reward function [10]. This involves subtracting
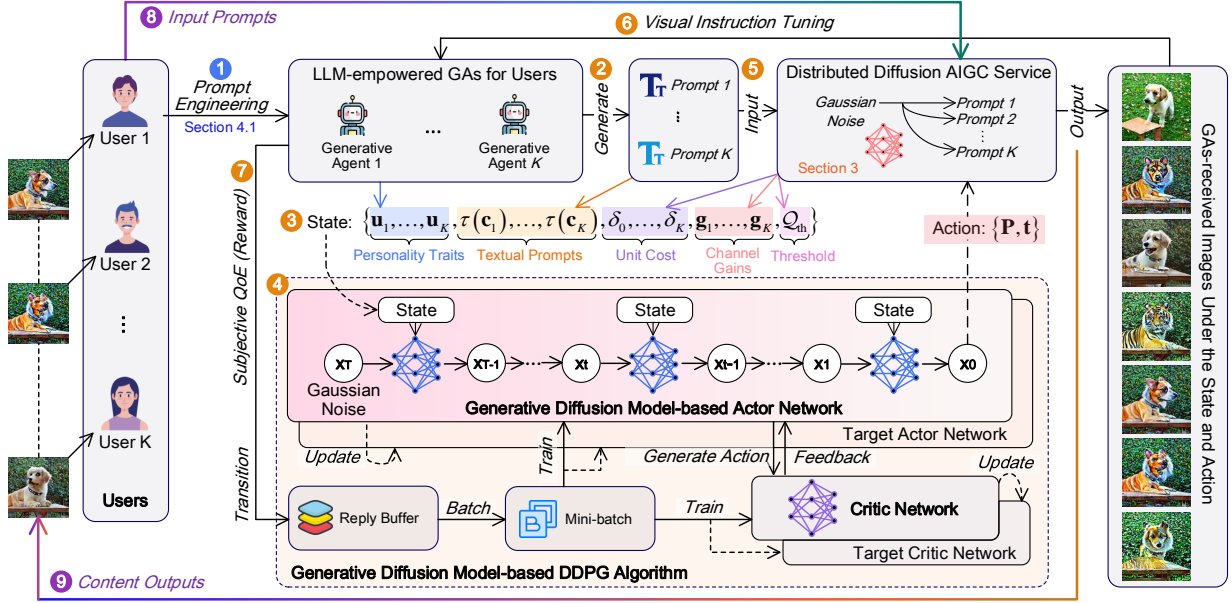
Fig. 7. The GDM-aided DDPG with LLMs interaction. Initially, users use prompts to customize LLM-empowered generative agents for personality simulation (**Step 1**). In **Steps 2 to 7** within the RLLI framework, generative agents generate prompts that, along with channel conditions and other environmental factors, form the *state* (**Step 3**). Actions are then generated through a GDM-based actor network (**Step 4**) and images are created via our proposed distributed diffusion AIGC framework. Subsequently, the generative agents use these images to generate QoE, providing feedback that serves as a reward for G-DDPG training (**Step 7**), cycling back to **Step 2** for iterative improvement. Upon finalizing the training, users request image generation (**Step 8**), and the trained G-DDPG along with the distributed diffusion AIGC model generates images aimed at maximizing the users' subjective QoE.

penalty terms for any constraint violations as

$$r = \sum_{k=1}^{K} \mathcal{Q}_k - \lambda_1 \sum_{k=1}^{K} \max\left(0, \delta_k t_k - E_{T_k}\right)$$
$$- \lambda_2 \sum_{k=1}^{K} \max\left(0, \mathcal{Q}_k - \mathcal{Q}_{\text{th}}\right)$$
$$- \lambda_3 \max\left(0, \delta_0 t_0 + \beta \sum_{k=1}^{K} P_k - E_{\text{T}}\right). \quad (27)$$

The penalties ensure that G-DDPG model learns the significance of constraints while facilitating exploration within the feasible solution space. The coefficients for these penalties can be tuned to balance the trade-off between exploration and adherence to the constraints.

Networks. The network architecture in G-DDPG comprises actor A_η and critic Q_v networks, alongside their corresponding target networks $A_{\eta'}$ and $Q_{v'}$. The GDM-based actor network responsible for generating actions and the critic network for evaluating actions. The target networks provide tempered, delayed targets, which help in stabilizing the training updates. The actor network's parameters are updated to maximize the expected reward, while the critic network's parameters are adjusted to minimize the error between the predicted and actual rewards. Specifically, the training loss for the actor network is given by

$$\arg\min_{A_\eta} \mathcal{L}_A(\eta) = -\mathbb{E}_{\boldsymbol{a} \sim A_\eta}\left[Q_v\left(\boldsymbol{s}, \boldsymbol{a}\right)\right]. \quad (28)$$

The critic network loss can be expressed as

$$\arg\min_{Q_v} \mathcal{L}_Q(v) = \mathbb{E}_{\boldsymbol{a} \sim \eta_\theta}\left[\left(Q_v\left(\boldsymbol{s}, \boldsymbol{a}\right) - r\right)^2\right], \quad (29)$$

where r is the actual Q-value, i.e., reward, obtained from the LLM-empowered generative agents after executing the action $\boldsymbol{a}$. The train and inference processes for our proposed G-DDPG with LLMs interaction algorithm is shown in **Algorithm 3**. During the training phase, the algorithm iterates over I episodes, each beginning with the GDM-based action generation with the current state as the condition and a noise process for exploration. The action is then executed within the proposed distributed GDM-based AIGC framework, and the subsequent reward is obtained from generative agents feedback and stored. A minibatch of experiences is sampled from the replay buffer to update the networks. Two target networks are updated with a soft copy of the weights, ensuring gradual learning. In the inference phase, the GDM-based actor network is utilized to generate optimal communication and computing resource allocation schemes in response to user prompts.

We then analyze the complexity of **Algorithm 3**. Let w_a and w_c denote the actor and critic networks' weight counts, respectively. Initialization has a complexity of $\mathcal{O}\left(2w_a + 2w_c\right)$. The complexity for action generation is augmented to $\mathcal{O}(Dw_a)$ per iteration due to D denoising steps in the action generation. The replay buffer operations remain $\mathcal{O}\left(1\right)$ for storage and $\mathcal{O}\left(N\right)$ for minibatch sampling. Updates to the critic and actor networks incur complexities of $\mathcal{O}\left(w_c\right)$ and $\mathcal{O}\left(w_a\right)$ per update, respectively. Target network updates are linear with respect to the number of parameters. Therefore, the training phase now demonstrates an adjusted

Algorithm 3 GDM-aided Double Deep Deterministic Policy Gradient Algorithm

---

Training Phase:

1: Initialize:
- Actor network A_θ and critic network Q_υ with random weights θ and υ, respectively
- Target networks $A_{\theta'}$ and $Q_{\upsilon'}$ with weights $\theta' \leftarrow \theta$ and $\upsilon' \leftarrow \upsilon$
- Replay buffer $\mathcal{B}$

2: Input prompts for K LLM-empowered generative agents as shown in Fig. 6

3: **for** each iteration $i = 1, 2, \ldots, I$ **do**

4:     Initialize a random process $\mathcal{N}$ for action exploration

5:     Observe the current state s

6:     **Generate action a according to (7) with s as the input and exploration noise**

7:     Execute action a and the distributed GDM-based AIGC framework, and observe reward r from generative agents according to (27)

8:     Store record (s, a, r) in $\mathcal{B}$

9:     Sample a random minibatch of N records (s, a, r) from $\mathcal{B}$

10:    Update the critic network (29)

11:    Update the actor network (28)

12:    Update the target networks:

$$\theta' \leftarrow \tau\theta + (1 - \tau)\theta'$$
$$\upsilon' \leftarrow \tau\upsilon + (1 - \tau)\upsilon'$$

13:    **Return**: The trained GDM-based actor network

14: **end for**

Inference Phase:

1: User upload their prompts and form the state s

2: Generate the optimal communication and computing resource allocation scheme a by using the trained GDM-based actor network

3: **Return**: a

---

computational complexity of $\mathcal{O}\left(I\left(Dw_a + w_c\right)\right)$. During the inference phase, generating the optimal resource allocation scheme through the trained actor network necessitates a complexity of $\mathcal{O}\left(w_a\right)$, assuming constant-time operations for reward observation and exploration noise generation.

5 EXPERIMENTS RESULTS

The central focus of this paper is the distributed GDM-based AIGC framework and the G-DDPG with LLMs interaction algorithm. Thus, our experiments are structured to investigate the following questions:

Q1) Is the proposed distributed GDM-based AIGC framework effective, with an emphasis on understanding an impact of wireless conditions and diffusion steps on its performance?

Q2) Is the RLLI framework is valid, particularly whether LLM-empowered generative agents can mimic human personalities to evaluate images accurately?

Q3) Is the G-DDPG with LLMs interaction algorithm is effective, specifically if it can converge fast and achieve high sum QoE feedback?

We first present the experimental setting and platform, and then answer the above questions through numerical evaluations. The code is available at https://github.com/HongyangDu/RLLI.

5.1 Experiments Setting

We initiated experiments where LLM-empowered generative agents are tasked with generating prompts for the training and testing of the distributed GDM-based AIGC framework and the G-DDPG with LLMs interaction algorithm. Specifically, we considered an environment with one server and three users, i.e., $K = 3$. The generative agents were first instructed to generate a set of 50 diverse objectives such as *"dog"*, *"cat"*, and *"tree"*. Subsequently, these generative agents combined the objectives to formulate prompts, e.g., *"dog under the tree"* and *"cat on the tree"*. These prompts were then used by the distributed GDM-based AIGC framework and the G-DDPG algorithm for final image generation. Then, generative agents, each embodying a distinct user personality, provided QoE feedback on image quality, which was used for further G-DDPG model training.

The experimental platform is built on a generic Ubuntu 20.04 system, powered by an AMD Ryzen Threadripper PRO 3975WX 32-Core CPU, and equipped with three NVIDIA RTX A5000 GPUs.

5.2 Experiments Performance Analysis

5.2.1 For **Q1**: Effectiveness of the Distributed GDM-based AIGC Framework

The distributed GDM-based AIGC framework optimizes energy usage by allocating denoising steps among the edge server and user devices while ensuring effective content generation. For ease of presentation, we consider two user devices with two different prompts. Specifically, *Device 1* has *Prompt 1*: *"A tiger sits in front of a bush"* and *Device 2* requires *Prompt 2*: *"A dog sits in front of a bush"*. The server initially executes t_0 denoising steps towards *Prompt 1*, and then the two devices separately perform t_1 and t_2 denoising steps, respectively.

Diverse power allocation strategies lead to various BEPs, impacting the quality of received data. Fig. 8 examines the impact of different BEP on image quality at *Device 1*. Our analysis yields two important insights: First, the user-side subsequent denoising process can mitigate the impact of bit errors, showing the framework's capacity to handle significant losses in wireless transmission. When the BEP is below 6%, the human-perceived image quality at *Device 1* remains basically unchanged. Second, excessively high BEP impairs the generative results because semantic information in intermediate denoised results significantly deviates due to bit errors and cannot be fully recovered through further denoising. This is evident when the BEP exceeds 10%, where noticeable artifacts appear in the images. Additionally, we employed generative agents to simulate users with different personalities and provide the QoE. The assessment by generative agents aligns with human visual perception, confirming that the framework has a high tolerance for bit errors but there exists a threshold that should not be exceeded.
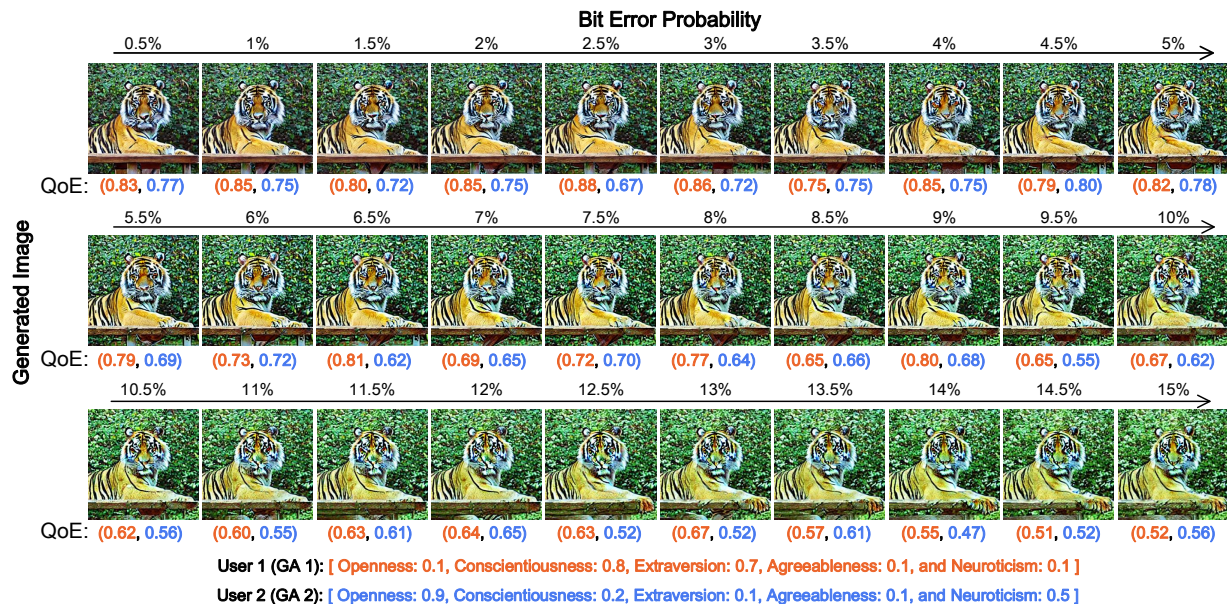
Fig. 8. Images generated at *Device 1* and corresponding generative agents evaluations under varying BEP from 0.5% to 15% within the proposed distributed GDM-based AIGC framework, considering 4 denoising steps at the edge server and 6 denoising steps at *Device 1*.

Fig. 9. Images generated at *Device 2* and corresponding generative agent evaluations under varying the denoising steps at the Server and *Device 2* within a distributed GDM-based AIGC Framework, the proposed distributed diffusion model-based AIGC framework, considering the BEP is 3%.

The insights from Fig. 8 highlight the crucial role of communications resource allocation. Building on this, Fig. 9 delves into the computing resource allocation, i.e., the setting of diffusion steps across network devices, and its impact on our distributed GDM-based AIGC framework. As shown in Fig. 9, we can observe that an increased number of denoising steps in the server, i.e., t_0, enhances the *"tiger"* semantics in the intermediate denoised results, influencing *Device 2*'s final output. For example, when $t_0 = 2$ and $t_2 > 4$, the generated dog image on *Device 2* barely exhibits tiger characteristics. However, if $t_0 = 3$, the generated dog on *Device 2* is free of tiger features only when $t_2 > 6$. With $t_0 = 4$, the generated dog on *Device 2* consistently displays tiger-like traits, such as stripes and coloration. Additionally, a minimum threshold of computing resources is essential; otherwise, the generated images lack distinctiveness, resulting in poor QoE. Furthermore, we observe that the semantic fusion of image content has varied effects on users with different personalities. For cases where $t_2 = 8$ with different t_0 settings, users with high *agreeableness* might favor a non-threatening dog. Consequently, the highest QoE is observed when $t_0 = 2$. Conversely, users with lower *agreeableness* and higher *openness* may favor a dog with tiger-like novelty, yielding the highest QoE when $t_0 = 4$.

For energy costs, we consider a general example with a typical smartphone processor in 2-nd user device, e.g., Qualcomm Snapdragon 870 processor [17]. As shown in Fig. 9, three steps are reduced in the image generation. If we consider that each step consumes around 1 to 2 milliwatt-hours (mWh), i.e., a plausible range for contemporary smartphone CPUs, the removal of three denoising steps could yield energy savings of 3 to 6 mWh per exe-
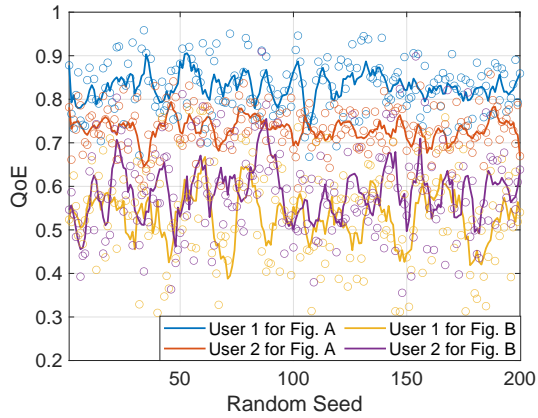
Fig. 10. The QoE feedback for generative agents when they evaluate subfigures A and B from Fig. 9, where the settings of GA1 and GA2 are *[Openness: 0.1, Conscientiousness: 0.8, Extraversion: 0.7, Agreeableness: 0.8, and Neuroticism: 0.1]* and *[Openness: 0.9, Conscientiousness: 0.2, Extraversion: 0.1, Agreeableness: 0.1, and Neuroticism: 0.5]*, respectively.
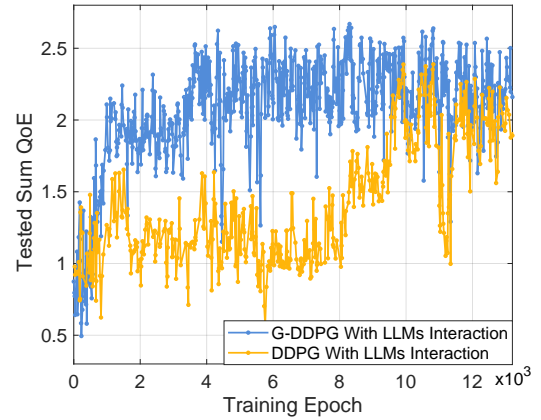
Fig. 11. Test reward curves of G-DDPG and DDPG [47] with LLMs interaction methods, where $K = 3$, $\delta_0 = 0.5$, $\delta_1 = \delta_2 = \delta_3 = 1$, $E_1 = E_2 = E_3 = 8$, $\mathcal{Q}_{\text{th}} = 0.6$, $\beta = 0.1$, $E_{\text{T}} = 20$, learning rate $= 10^{-4}$, $\boldsymbol{g}_i \sim$ Fisher–Snedecor $\mathcal{F}$ distribution with the fading severity parameter is 2 and shadowing amount parameter is 1.5 [51].

cution of the model. Such a reduction would amount to an approximate 20% to 40% decrease in energy consumption for each full cycle of the GDM, relative to the original number of steps. This example highlights the potential for enhancing energy efficiency in AIGC processes on mobile platforms. Nonetheless, accurate quantification of energy savings necessitates specific empirical measurements with the designated hardware and the precise GAI model.

5.2.2 For **Q2**: Effectiveness of the RLLI Framework

LLM-empowered generative agents have demonstrated their effectiveness in evaluating a variety of images, as evidenced in Figs. 8 and 9. It is important to note that with a fixed random seed in VIT and LLM setting, generative agents can produce the same feedback. Without a fixed seed, a crucial aspect of GA feedback for RL is the stability of the evaluation aligned with the personality traits setting of the generative agents. As shown in Fig. 10, we use two generative agents with different personality settings to evaluate subfigures A and B from Fig. 9 across 200 different random seeds. We observe that, despite some fluctuations, there is a discernible clustering of feedback QoE values by a GA for a particular image, suggesting that the generative agents' assessments are consistent with their personality traits settings. Furthermore, when the image quality is high, as in subfigure A, feedback from both generative agents is more stable with less variability. In contrast, lower-quality images result in greater fluctuations in GA feedback. We further verify the effectiveness of the RLLI by subsequent G-DDPM training and inference.

5.2.3 For **Q3**: Effectiveness of the G-DDPG with LLMs Interaction Algorithm

In Fig. 11, we present the training convergence of G-DDPG with LLMs interaction, in comparison with the DDPG algorithm under the RLLI framework. While the QoE test curves for both algorithms improve over time, G-DDPG achieves a faster convergence and a higher final sum QoE. This superior performance is attributed to the robust modeling capability of the GDM, which facilitates the DDPG

algorithm's accelerated learning of the environment and convergence [11]. Subsequently, we employed the trained model to generate joint communication and computing resource allocation schemes for the case considered in Section 5.2.1. To obtain more insights, Figs. 13 and 14 illustrate the QoE feedback from two generative agents across various resource allocation schemes and BEP values. A consistent observation is that irrespective of computing resource allocation, insufficient communications resources lead to a higher BEP and result in diminished peak QoE values. As shown in Fig. 13, where both *Device 1* and the *Server* perform the same prompt, we observe that larger values of t_0 and t_1, which corresponds to a larger number of total denoising steps towards *Prompt 1*, yield higher QoE feedback from the GA. However, as shown in Fig. 14, since *Device 2* and the *Server* execute different prompts, increasing denoising steps at the *Server* does not always enhance QoE, as semantic integration may compromise image quality to some extent. In this case, peak QoE values are achieved when t_0 is moderate, and t_2 is sufficient. Furthermore, the red pentagram marks the joint communication and computing resource allocation scheme under G-DDPM. As shown in Fig. 12, we obtain $t_0 = 3$, $t_1 = 5$, $t_2 = 7$, and the transmission power from the *Server* to *Device 1* and *Device 2* are 18 and 21 dBW, respectively. This leads that *Device 1*'s BEP being 5% and *Device 2*'s BEP being 3%, as shown in Figs. 13 and 14. Besides increased denoising steps, more communications resources are allocated to *Device 2* to minimize bit error in the interrupted results, thus reducing the complexity of directional semantic changes in the denoising process. Consequently, the maximum total QoE is obtained.

6 CONCLUSION

We have introduced a distributed GDM-based AIGC framework that enhances energy efficiency and maximize the subjective QoE by the proposed IAI method, i.e., RLLI algorithm. Through the novel restructuring of the denoising process in GDMs, we facilitated resource saving by reducing the total executed denoising steps while accommodating user requirements by leveraging shared diffusion process
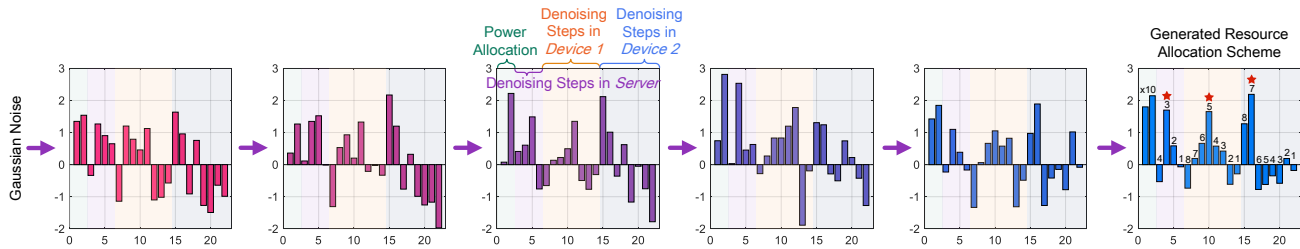
Fig. 12. The communication and computing resource allocation scheme in each denoising step of the inference process.
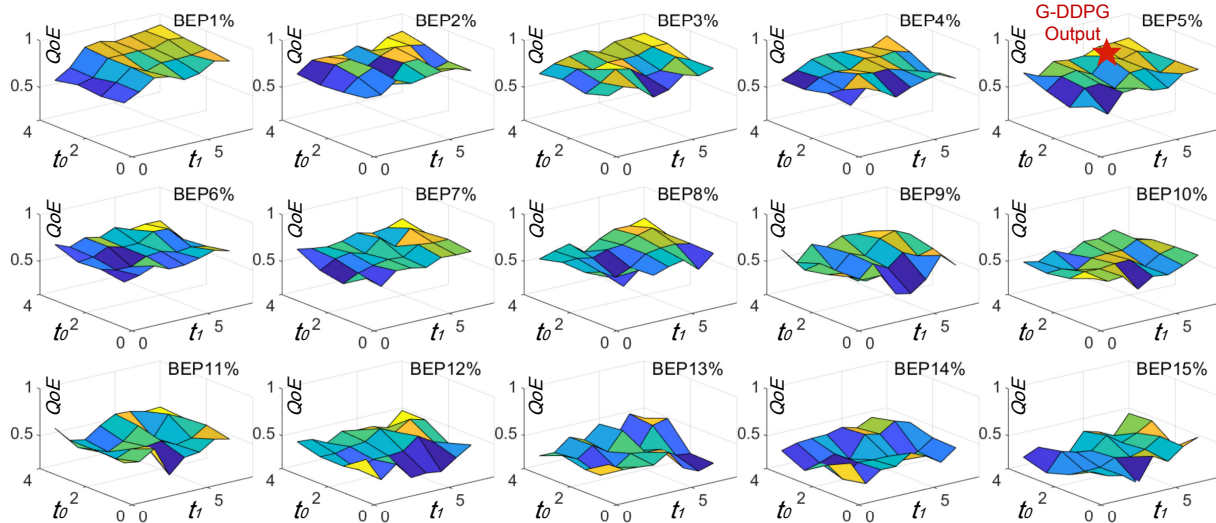

Fig. 13. GA's QoE feedback at *Device 1* under varying BEP from 0.5% to 15% and different denoising steps within the proposed distributed GDM-based AIGC framework.

for semantically similar prompts. The proposed RLLI algorithm is an interactive AI method, which utilizes LLM-empowered generative agents to provide subjective and real-time QoE feedback for AI-based resource allocation model training. Specifically, our proposed G-DDPG with LLMs interaction algorithm optimizes communication and computing resource allocation by considering user personalities and dynamic conditions. The simulations demonstrated a substantial improvement in the sum QoE, up to 15%, over conventional DDPG methods. Future research directions include:

- *Caching Mechanism.* Developing a caching mechanism for intermediate denoised results, enabling server-side computational reuse by delivering cached outcomes to users when their prompts closely align with those in the cache.
- *Dataset for Generative Agents.* Establishing a dataset through surveys with natural human users to improve the simulation of user preferences by LLM-empowered generative agents, thereby enhancing the accuracy of subjective QoE assessments.
- *Style-controllable AIGC.* Expanding the distributed AIGC framework to train more general style-controllable AIGC models, which, through interactive AI, can cater to human users' preferences with higher personalization.

REFERENCES

[1] X. Guo and L. Zhao, "A systematic survey on deep generative models for graph generation," *IEEE Trans. Pattern Anal. Mach. Intell.*, vol. 45, no. 5, pp. 5370–5390, May 2022.

[2] H. Du, Z. Li, D. Niyato, J. Kang, Z. Xiong, D. I. Kim *et al.*, "Enabling AI-generated content (AIGC) services in wireless edge networks," *IEEE Wireless Mag.*, to appear, 2023.

[3] B. D. Lund and T. Wang, "Chatting about ChatGPT: how may AI and GPT impact academia and libraries?" *Library Hi Tech News*, vol. 40, no. 3, pp. 26–29, Mar. 2023.

[4] S. AI, "Stable diffusion," https://stability.ai/.

[5] F.-A. Croitoru, V. Hondru, R. T. Ionescu, and M. Shah, "Diffusion models in vision: A survey," *IEEE Trans. Pattern Anal. Mach. Intell.*, to appear, 2023.

[6] S. Amershi, D. Weld, M. Vorvoreanu, A. Fourney, B. Nushi, P. Collisson, J. Suh, S. Iqbal, P. N. Bennett, K. Inkpen *et al.*, "Guidelines for human-AI interaction," in *Proc. 2019 Chi Conf. Human Fact. Comput. Syst.*, 2019, pp. 1–13.

[7] R. W. Picard, E. Vyzas, and J. Healey, "Toward machine emotional intelligence: Analysis of affective physiological state," *IEEE Trans. Pattern Anal. Mach. Intell.*, vol. 23, no. 10, pp. 1175–1191, Oct. 2001.

[8] P. Juluri, V. Tamarapalli, and D. Medhi, "Measurement of quality of experience of video-on-demand services: A survey," *IEEE Commun. Surv. Tut.*, vol. 18, no. 1, pp. 401–418, Jan. 2015.

[9] H. Du, J. Liu, D. Niyato, J. Kang, Z. Xiong, J. Zhang, and D. I. Kim, "Attention-aware resource allocation and QoE analysis for metaverse xURLLC services," *IEEE J. Selec. Areas Commun.*, vol. 41, no. 7, Jul. 2023.

[10] N. C. Luong, D. T. Hoang, S. Gong, D. Niyato, P. Wang, Y.-C. Liang, and D. I. Kim, "Applications of deep reinforcement learning in communications and networking: A survey," *IEEE Commun. Surv. Tut.*, vol. 21, no. 4, pp. 3133–3174, Apr. 2019.

[11] H. Du, R. Zhang, Y. Liu, J. Wang, Y. Lin, Z. Li, D. Niyato, J. Kang, Z. Xiong, S. Cui *et al.*, "Beyond deep reinforcement learning: A
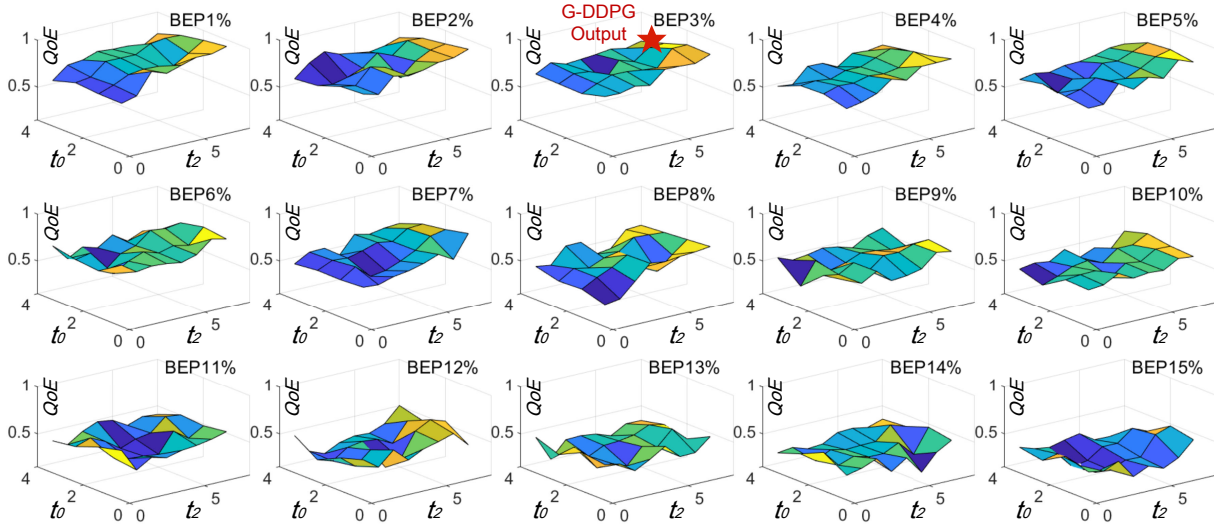
Fig. 14. GA's QoE feedback at *Device 2* under varying BEP from 0.5% to 15% and different denoising steps within the proposed distributed GDM-based AIGC framework.

tutorial on generative diffusion models in network optimization," arXiv preprint arXiv:2308.05384, 2023.

[12] P. Liu, W. Yuan, J. Fu, Z. Jiang, H. Hayashi, and G. Neubig, "Pre-train, prompt, and predict: A systematic survey of prompting methods in natural language processing," *ACM Comput. Surv.*, vol. 55, no. 9, pp. 1–35, Sep. 2023.

[13] M. Xu, H. Du, D. Niyato, J. Kang, Z. Xiong, S. Mao, Z. Han, A. Jamalipour, D. I. Kim, V. Leung *et al.*, "Unleashing the power of edge-cloud generative AI in mobile networks: A survey of AIGC services," arXiv preprint arXiv:2303.16129, 2023.

[14] S. Dang, O. Amin, B. Shihada, and M.-S. Alouini, "What should 6G be?" *Nat. Electron.*, vol. 3, no. 1, pp. 20–29, Jan. 2020.

[15] X. Ma, G. Fang, and X. Wang, "LLM-Pruner: On the structural pruning of large language models," arXiv preprint arXiv:2305.11627, 2023.

[16] B.-K. Kim, H.-K. Song, T. Castells, and S. Choi, "On architectural compression of text-to-image diffusion models," arXiv preprint arXiv:2305.15798, 2023.

[17] H. Du, R. Zhang, D. Niyato, J. Kang, Z. Xiong, D. I. Kim, X. S. Shen, and H. V. Poor, "Exploring collaborative distributed diffusion-based AI-generated content (AIGC) in wireless networks," *IEEE Netw.*, no. 99, pp. 1–8, 2023.

[18] J. Ho, A. Jain, and P. Abbeel, "Denoising diffusion probabilistic models," *Adv. Neural Inf. Process. Syst.*, vol. 33, pp. 6840–6851, 2020.

[19] J. Ho, T. Salimans, A. Gritsenko, W. Chan, M. Norouzi, and D. J. Fleet, "Video diffusion models," arXiv:2204.03458, 2022.

[20] X. Li, J. Thickstun, I. Gulrajani, P. S. Liang, and T. B. Hashimoto, "Diffusion-lm improves controllable text generation," *Adv. Neural Inf. Process. Syst.*, vol. 35, pp. 4328–4343, 2022.

[21] M. Reid, V. J. Hellendoorn, and G. Neubig, "Diffuser: Diffusion via edit-based reconstruction," *Proc. Int. Conf. Learn. Represent.*, 2023.

[22] R. Huang, Z. Zhao, H. Liu, J. Liu, C. Cui, and Y. Ren, "Prodiff: Progressive fast diffusion model for high-quality text-to-speech," in *Proc. ACM Int. Conf. Multimedia*, 2022, pp. 2595–2605.

[23] Z. Kong, W. Ping, J. Huang, K. Zhao, and B. Catanzaro, "DiffWave: A versatile diffusion model for audio synthesis," in *Proc. Int. Conf. Learn. Represent.*, 2021.

[24] C. Niu, Y. Song, J. Song, S. Zhao, A. Grover, and S. Ermon, "Permutation invariant graph generation via score-based generative modeling," in *Proc. Int. Conf. Artif. Intell. Stat.*, 2020, pp. 4474–4484.

[25] M. A. Ketata, C. Laue, R. Mammadov, H. Stark, M. Wu, G. Corso, C. Marquet, R. Barzilay, and T. S. Jaakkola, "DiffDock-PP: Rigid protein-protein docking with diffusion models," in *Proc. Int. Conf. Learn. Represent.*, 2023.

[26] L. Li, H. Zhu, S. Zhao, G. Ding, and W. Lin, "Personality-assisted multi-task learning for generic and personalized image aesthetics assessment," *IEEE Trans. Image Process.*, vol. 29, pp. 3898–3910, Jan. 2020.

[27] G. Saucier and L. R. Goldberg, "What is beyond the Big Five?" *J. Pers.*, vol. 66, pp. 495–524, 1998.

[28] M. Cristani, A. Vinciarelli, C. Segalin, and A. Perina, "Unveiling the multimedia unconscious: Implicit cognitive processes and multimedia content analysis," in *Proc. ACM Int. Conf. Multimedia*, 2013, pp. 213–222.

[29] J. Wang, Y. Liang, F. Meng, H. Shi, Z. Li, J. Xu, J. Qu, and J. Zhou, "Is ChatGPT a good NLG evaluator? A preliminary study," arXiv preprint arXiv:2303.04048, 2023.

[30] H. Lee, S. Phatale, H. Mansoor, K. Lu, T. Mesnard, C. Bishop, V. Carbune, and A. Rastogi, "Rlaif: Scaling reinforcement learning from human feedback with AI feedback," arXiv preprint arXiv:2309.00267, 2023.

[31] C. Ziems, W. Held, O. Shaikh, J. Chen, Z. Zhang, and D. Yang, "Can large language models transform computational social science?" arXiv preprint arXiv:2305.03514, 2023.

[32] X. Wang, Y. Fei, Z. Leng, and C. Li, "Does role-playing chatbots capture the character personalities? Assessing personality traits for role-playing chatbots," *arXiv preprint arXiv:2310.17976*, 2023.

[33] J. Sohl-Dickstein, E. Weiss, N. Maheswaranathan, and S. Ganguli, "Deep unsupervised learning using nonequilibrium thermodynamics," in *Proc. Int. Conf. Mach. Learn.* PMLR, 2015, pp. 2256–2265.

[34] Y. Song and S. Ermon, "Generative modeling by estimating gradients of the data distribution," *Adv. Neural Inf. Process. Syst.*, vol. 32, 2019.

[35] Y. Song, J. Sohl-Dickstein, D. P. Kingma, A. Kumar, S. Ermon, and B. Poole, "Score-based generative modeling through stochastic differential equations," arXiv preprint arXiv:2011.13456, 2020.

[36] D. Kingma, T. Salimans, B. Poole, and J. Ho, "Variational diffusion models," *Adv. Neural Inf. Process. Syst.*, vol. 34, pp. 21 696–21 707, 2021.

[37] O. Ronneberger, P. Fischer, and T. Brox, "U-net: Convolutional networks for biomedical image segmentation," in *In MICCAI (3), volume 9351 of Lecture Notes in Computer Science*. Springer, 2015, pp. 234–241.

[38] J. Gauthier, "Conditional generative adversarial nets for convolutional face generation," *Class project for Stanford CS231N: convolutional neural networks for visual recognition, Winter semester*, vol. 2014, no. 5, p. 2, 2014.

[39] K. Sohn, H. Lee, and X. Yan, "Learning structured output representation using deep conditional generative models," *Adv. Neural Inf. Process. Syst.*, vol. 28, 2015.

[40] S. Reed, Z. Akata, X. Yan, L. Logeswaran, B. Schiele, and H. Lee, "Generative adversarial text to image synthesis," in *Proc. Int. Conf. Mach. Learn.* PMLR, 2016, pp. 1060–1069.

[41] T. Park, M.-Y. Liu, T.-C. Wang, and J.-Y. Zhu, "Semantic image synthesis with spatially-adaptive normalization," in *Proc. IEEE Conf. Comput. Vis. Pattern Recognit.*, 2019, pp. 2337–2346.

[42] P. Isola, J.-Y. Zhu, T. Zhou, and A. A. Efros, "Image-to-image translation with conditional adversarial networks," in *Proc. IEEE Conf. Comput. Vis. Pattern Recognit.*, 2017, pp. 1125–1134.

[43] H. Ko, S. Lee, Y. Park, and A. Choi, "A survey of recommendation systems: Recommendation models, techniques, and application fields," *Electronics*, vol. 11, no. 1, p. 141, Jan. 2022.

[44] H. Liu, C. Li, Q. Wu, and Y. J. Lee, "Visual instruction tuning," arXiv preprint arXiv:2304.08485, 2023.

[45] H. Touvron, T. Lavril, G. Izacard, X. Martinet, M.-A. Lachaux, T. Lacroix, B. Rozière, N. Goyal, E. Hambro, F. Azhar *et al.*, "Llama: Open and efficient foundation language models," arXiv preprint arXiv:2302.13971, 2023.

[46] S. Griffith, K. Subramanian, J. Scholz, C. L. Isbell, and A. L. Thomaz, "Policy shaping: Integrating human feedback with reinforcement learning," *Adv. Neural Inf. Process. Syst.*, vol. 26, 2013.

[47] T. P. Lillicrap, J. J. Hunt, A. Pritzel, N. Heess, T. Erez, Y. Tassa, D. Silver, and D. Wierstra, "Continuous control with deep reinforcement learning," arXiv preprint arXiv:1509.02971, 2015.

[48] L. Ale, S. A. King, N. Zhang, A. R. Sattar, and J. Skandaraniyam, "D3PG: Dirichlet DDPG for task partitioning and offloading with constrained hybrid action space in mobile-edge computing," *IEEE Internet Things J.*, vol. 9, no. 19, pp. 19 260–19 272, 2022.

[49] R. Zhang, K. Xiong, Y. Lu, P. Fan, D. W. K. Ng, and K. B. Letaief, "Energy efficiency maximization in RIS-assisted SWIPT networks with RSMA: A PPO-based approach," *IEEE J. Sel. Areas Commun.*, vol. 41, no. 5, pp. 1413–1430, May 2023.

[50] H. Hasselt, "Double Q-learning," *Adv. Neural Inf. Process. Syst.*, vol. 23, 2010.

[51] S. K. Yoo, S. L. Cotton, P. C. Sofotasios, M. Matthaiou, M. Valkama, and G. K. Karagiannidis, "The Fisher-Snedecor { distribution: A simple and accurate composite fading model," *IEEE Commun. Lett.*, vol. 21, no. 7, pp. 1661–1664, Jul. 2017.